

Dark Matter Annihilation in Substructures Revised

Lidia Pieri^{1,2}, Gianfranco Bertone³ and Enzo Branchini⁴

¹*Istituto Nazionale di Astrofisica - Osservatorio di Padova,
Via Colson 3, 35122 Padova, Italy*

²*Istituto Nazionale di Fisica Nucleare - Sezione di Padova,
Via Marzolo 8, 35131 Padova, Italy*

³*Institut d'Astrophysique de Paris, UMR 7095-CNRS,
Université Pierre et Marie Curie, 98bis boulevard Arago, 75014 Paris, France*

⁴*Department of Physics, Università di Roma Tre,
Via della Vasca Navale 84, 00146, Rome, Italy*

27 October 2018

ABSTRACT

Upcoming γ -ray satellites will search for Dark Matter annihilations in Milky Way substructures (or ‘clumps’). The prospects for detecting these objects strongly depend on the assumptions made on the distribution of Dark Matter in substructures, and on the distribution of substructures in the Milky Way halo. By adopting simplified, yet rather extreme, prescriptions for these quantities, we compute the number of sources that can be detected with upcoming experiments such as GLAST, and show that, for the most optimistic particle physics setup ($m_\chi = 40$ GeV and annihilation cross section $\sigma v = 3 \times 10^{-26} \text{ cm}^3 \text{ s}^{-1}$), the result ranges from zero to \sim hundred sources, all with mass above $10^5 M_\odot$. However, for a fiducial DM candidate with mass $m_\chi = 100$ GeV and $\sigma v = 10^{-26} \text{ cm}^3 \text{ s}^{-1}$, at most a handful of large mass substructures can be detected at 5σ , with a 1-year exposure time, by a GLAST-like experiment. Scenarios where micro-clumps (i.e. clumps with mass as small as $10^{-6} M_\odot$) can be detected are severely constrained by the diffuse γ -ray background detected by EGRET.

1 INTRODUCTION

Indirect Dark Matter [DM] searches are based on the detection of secondary particles and radiation produced by the self-annihilation of DM particles (Bergström 2000, Bertone et al. 2005a).

Although the predicted annihilation flux is typically affected by large astrophysical uncertainties, the detection of multiwavelength photons, neutrinos or anti-matter from regions with high DM density would be of paramount importance for the identification of DM particles. In fact, accelerator searches of Physics beyond the Standard Model at the Large Hadron Collider, will not necessarily unveil the nature of DM, even if new particles are discovered, due to the difficulties associated with the reconstruction of the cosmological abundance of the newly discovered particles (e.g. Baltz et al. 2006a, Nojiri et al. 2005). At the same time, DM particles could have small enough couplings to nucleons, to lead to null searches in direct detection experiments (see e.g. Muñoz 2003 and references therein).

In the framework of indirect DM searches, several strategies have thus been devised, in order to obtain *conclusive* evidence from astrophysical observations. For instance, one could search for peculiar features, such as lines or sharp cut-offs, in the γ -ray spectrum. Although for commonly studied DM candidates there are no tree level processes for direct annihilation into photons, loop-level processes to $\gamma\gamma$ and γZ^0 may produce detectable lines at an energy equal to

the DM particle mass (see e.g. Bergström & Ullio 1997, Ullio & Bergström 1998, Gounaris et al. 2003, Bergström et al. 2005a). Other spectral features may help distinguishing the DM annihilation signal from ordinary astrophysical sources (Bergström et al. 2005b, Bergström et al. 2005c; see also the discussion in Baltz et al. 2006b). Alternatively, one can search for annihilation radiation from regions characterized by large concentrations of DM, but very few baryons, such as DM substructures in the Milky Way [MW hereafter] halo, including dwarf galaxies (Baltz et al. 2000, Tasitsiomi et al. 2003, Pieri & Branchini 2003, Evans et al. 2003, Tyler 2002, Colafrancesco et al. 2007, Bergström & Hooper 2006) and DM mini-spikes around Intermediate Mass Black Holes (Bertone 2006, Bertone et al. 2005b, Horiuchi & Ando 2006, Fornasa et al. 2007, Brun et al. 2007). Finally, DM annihilation features can be detected in the energy spectrum and angular distribution of the cosmic γ -ray background (Bergström, Edsjö & Ullio 2001, Ando & Komatsu 2006).

In the popular Cold DM scenario, gravitational instabilities lead to the formation of a wealth of virialized structures, the DM haloes, spanning a huge range of masses, from the largest clusters of galaxies of $\sim 10^{15} M_\odot$ down to Earth-size clumps of $\sim 10^{-6} M_\odot$ (Green et al. 2004, Green et al. 2005). Although the detectability of individual DM substructures, or “clumps” has been widely discussed in literature, the number of detectable clumps with a GLAST-like experiment, at 5σ in 1 year and for a WIMP DM particle is highly uncertain, ranging from $\lesssim 1$ (Koushiappas

et al. 2004) to more than 50 (Baltz 2006b) for large mass haloes, while for microhaloes (i.e. clumps with a mass as small as $10^{-6}M_{\odot}$) the predictions range from no detectable objects (Pieri et al. 2005) to a large number of detectable objects, with a fraction of them exhibiting a large proper motion (Koushiappas 2006). The apparent inconsistency of the results published so far, is actually due to the different assumptions that different groups adopt for the physical quantities that regulate the number and the annihilation "brightness" of DM clumps. In particular, even in the context of the benchmark density profile introduced by Navarro, Frenk and White 1996 [NFW], the results crucially depend on the substructures mass function, their distribution within the halo host and their virial concentration $c(M, z)$ which is a function of mass and of collapse redshift of DM clumps.

The paper is organized as follows: in Sec. 2, we describe the model we have adopted for the smooth component of the Galactic halo, and introduce the eight different models for DM substructures that will be discussed in the rest of the paper. In Sec.3 we estimate the contribution to the γ -ray flux due to the smooth Galactic halo, unresolved DM clumps, and resolved (detectable) clumps. In Sec.4, we study the prospects for detection of substructures with upcoming experiments such as GLAST, and in Sec.5 we discuss the results and present our conclusions.

2 MODELING THE GALACTIC HALO AND ITS SUBSTRUCTURES

High resolution N-body experiments indicate that a large fraction of the mass within Dark Matter haloes is in the form of virialized subhaloes in all resolved mass scales. Their annihilation signal, which adds to that of the smooth Galactic component could be significant (Stoher et al. 2003, Diemand et al. 2006, Diemand et al. 2007a). A precise modeling of both the smooth DM distribution (the diffuse galactic component) and the subhalo population within (the clumpy component) is therefore mandatory to assess the possibility of detecting DM subhaloes through their annihilation signal. High resolution numerical simulations enable to study gravitationally bound subhaloes with $M_{SH} \geq 10^{-6} M_{\text{Host}}$, where M_{Host} is the mass of the host, and therefore cannot resolve substructures in a MW-size halo all the way down to $\sim 10^{-6}M_{\odot}$. In fact, the smallest substructures of interest must be studied within host haloes with mass $\sim 0.1M_{\odot}$ and only at very large redshift (Diemand et al. 2006). At $z = 0$ and within a MW-host the smallest subhaloes that we resolve have masses $\geq 10^6 M_{\odot}$ (Diemand et al. 2007a) As a consequence the spatial distribution, mass function and internal structure of Galactic subhaloes can only be interpolated from the results of several numerical experiments spanning a large range of masses and redshifts using self-similarity arguments. This interpolation is affected by a number of uncertainties that we account for by exploring different models that meet the numerical constraints.

2.1 The diffuse Galactic component

The recent "Via Lactea" high resolution simulation (Diemand et al. 2007a) shows that the density profile of a MW-sized DM halo is consistent to within 10% with the NFW

profile that we adopt here:

$$\begin{aligned} \rho_{\chi}(r) &= \frac{\rho_s}{\left(\frac{r}{r_s}\right) \left(1 + \frac{r}{r_s}\right)^2}, & r > r_{min} \\ \rho_{\chi}(r) &= \rho_{\chi}(r_{min}), & r \leq r_{min} \end{aligned} \tag{1}$$

where r is the distance from the halo center. This profile depends on two free parameters, the scale density, ρ_s , and the scale radius, r_s , that are related to each other by the virial mass of the halo, M_h . The latter is the mass enclosed in a sphere with radius r_{vir} within which the mean density is 200 times above critical. A different definition of r_{vir} would not change the DM profile nor our results. Finally, we adopt a small core radius $r_{min} = 10^{-8}$ kpc.

An important shape parameter that characterizes the density profile is the virial concentration defined as the ratio between the virial radius and the scale radius, $c \equiv r_{vir}(M_h)/r_s$. Theoretical considerations corroborated by numerical experiments show that a relation exists between the mass of a halo, its collapse redshift, z_{coll} , and concentration parameter c . The collapse redshift is defined as in Bullock et al. 2001, as the epoch in which a mass scale M_h breaks into the nonlinear regime, i.e. when $\sigma(M_h)D(z_{coll}) \sim 1$, where $\sigma(M_h)$ is the present linear theory amplitude of mass fluctuation on the scale M_h and $D(z_{coll})$ is the linear theory growth factor at the redshift z_{coll} . The two models proposed by Bullock et al. 2001 [B01] and Eke et al. 2001 [ENS01] are consistent for masses larger than $\sim 10^9 M_{\odot}$ and in this paper we use the concentration parameter by B01 to model the diffuse Galactic component. On the contrary, for smaller masses ENS and B01 predictions become very different and we will have to consider both of them to model the subhaloes annihilation signal.

Since a sizable fraction of the mass in the MW is in the form of virialized subhaloes, there is not a unique way to determine ρ_s , and r_s of the host MW halo. For this reason we adopted two different procedures. In the first one we have computed ρ_s , and r_s as if the total mass of the system, including the clumpy component, were in fact smoothly distributed in the Galactic halo. In the second we have considered the total mass of the system to determine the concentration parameter but have used the diffuse component alone to relate ρ_s to r_s . Having checked that both procedures give similar predictions for the probability of subhalo detection (Section 3), in the following we will only discuss models based on the second approach. For the Milky Way we have used a virial mass $M_h = 10^{12} M_{\odot}$ and a concentration parameter $c_{vir} \sim 9.8$.

2.2 The clumpy component

To account for the presence of a population of DM subhaloes and investigate their effect on the annihilation signal, we need to specify their mass spectrum, spatial distribution and density profile.

Subhalo Models				
Model name	$c(M)$		z_{coll}	c
	$> 10^4 M_\odot$	$10^{-6} M_\odot$	$10^{-6} M_\odot$	$10^{-6} M_\odot$
B_{ref,z_0}	B01	B01	0	63
B_{z_0}	B01	DMS05	0	80
$B_{z_0,5\sigma}$	B01	DMS05-5 σ	0	400
B_{ref,z_c}	B01	B01	B01	~ 3.7
B_{z_c}	B01	DMS05	DMS05	~ 1
$B_{z_c,5\sigma}$	B01	DMS05-5 σ	DMS05	~ 0.6
ENS_{z_0}	ENS01	DMS05	0	80
ENS_{z_c}	ENS01	DMS05	DMS05	~ 1

Table 1. Halo model parameters. Column 1: Model name. Column 2: Halo density profile for $M > 10^4 M_\odot$. Column 3: Halo density profile benchmark for $M = 10^{-6} M_\odot$, used as normalization. Column 4: Collapse redshift model, used as normalization. Column 5: Concentration parameter at $10^{-6} M_\odot$. For all the models we have adopted an NFW profile.

2.2.1 The Mass function and the Spatial Distribution of Clumps

High resolution N-body experiments show that the mass function of both isolated field haloes and subhaloes is well approximated by a power law

$$dn(M)/d\ln(M) \propto M^{-\alpha}, \quad (2)$$

with $\alpha = 1$, independently of the host halo mass, over the large redshift range $z = [0, 75]$, and mass intervals $M = [10^{-6}, 10^{10}] M_\odot$ (Jenkins et al. 2001, Moore et al. 2001, Diemand et al. 2004, Gao et al. 2005, Reed et al. 2005, Diemand et al. 2006). Self-similarity is preserved at the present epoch down to the smallest masses if subhaloes survive gravitational disturbances during early merger processes and late tidal disruption from stellar encounters.

Analytical arguments have been given against (Zhao et al. 2005) or in support of this hypothesis (Moore et al. 2005, Brezinsky et al. 2006). Moreover, currently resolved mass functions in numerical experiments suffer from dynamical friction at the high mass end which could steepen the halo mass function. Since changing the halo mass function slope might have a non-negligible impact on our analysis, we adopt a power-law index $\alpha = 1$ as a reference case but also explore two shallower subhalo mass functions with $\alpha = 0.9$ and $\alpha = 0.95$. All plots in this paper refer to the reference case $\alpha = 1$ and discuss the effect of adopting shallower slopes in the text.

As far as the spatial distribution of subhalos inside our Galaxy is concerned, we follow the indications of the numerical experiment of Reed et al. 2005 and assume that the subhalo distribution traces that of the underlying host mass from r_{vir} and down to a minimum radius, $r_{\text{min}}(M)$, within which subhaloes are efficiently destroyed by gravitational interactions. We explicitly assume spherical symmetry and we ignore the possibility, indicated by some numerical experiments, that the radial distribution of subhalos might be more extended than that of the dark matter.

Folding these indications together we model the number density of subhaloes per unit mass at a distance R from the GC as:

$$\rho_{sh}(M, R) = AM^{-2} \frac{\theta(R - r_{\text{min}}(M))}{(R/r_s^{MW})(1 + R/r_s^{MW})^2} M_\odot^{-1} \text{ kpc}^{-3}, \quad (3)$$

where r_s^{MW} is the scale radius of our Galaxy and the effect of tidal disruption is accounted for by the Heaviside step function $\theta(r - r_{\text{min}}(M))$. To determine the tidal radius, $r_{\text{min}}(M)$, we follow the Roche criterion and compute it as the minimum distance at which the subhalo self gravity at r_s equals the gravity pull of the halo host computed at the orbital radius of the subhalo. As a result $r_{\text{min}}(M)$ is an increasing function of the subhalo mass, implying that no subhaloes survive within $r_{\text{min}}(10^{-6} M_\odot) \sim 200$ pc.

To normalize eq. 3, we again refer to numerical simulations that show that [5-10]% of the MW mass is distributed in subhaloes with masses in the range $10^7 - 10^{10} M_\odot$ (Diemand et al. 2005, Diemand et al. 2007). In the following we use the optimistic value of 10 % and note that assuming 5%, instead, would decrease the probability of subhalo detection by a factor 2. With this normalization about 53% of the MW mass is condensed within $\sim 1.5 \times 10^{16}$ subhaloes with masses in the range $[10^{-6}, 10^{10}] M_\odot$, whose abundance in the solar neighborhood is remarkably high ($\sim 100 \text{ pc}^{-3}$). The remaining 47% constitutes the diffuse galactic component that is assumed to follow a smooth NFW profile. We do not account here for the presence of mass debris streams resulting from tidal stripping since these structures, characterized by a mild density contrast, would not contribute significantly to the annihilation flux.

2.2.2 Density Profile.

Finally, we need to specify the density profile for the substructures. Constraints from numerical models only applies to limited mass ranges at very different epochs. At $z = 0$ Diemand et al. 2007b find that the velocity profile of Galactic subhaloes above $4 \times 10^6 M_\odot$ in the ‘‘Via Lactea’’ simulation are well fitted by the NFW model. This result is also valid for the much smaller substructures with masses in the range $[10^{-6}, 4 \times 10^{-3}] M_\odot$ that populate a parent halo of $0.014 M_\odot$ at $z = 86$ (Diemand et al. 2006). A large fraction of these small substructures do not survive the early stage of hierarchical merging and late tidal interaction with stellar encounters (Zhao et al. 2005). The $\sim 10^{16}$ survivors suffer from significant mass loss. Presumably this modifies their original NFW density profile that, however, seems to be preserved in the innermost region where most of the annihilation signal originates from (Kazantzidis et al. 2004).

Yet these constraints from numerical experiments do not uniquely define the subhalo density profiles. Therefore, instead of relying on a single model profile we will explore several of them in an attempt of bracketing the theoretical uncertainties.

All models that we have considered, and that are listed in Table 1, assume that subhaloes have the same NFW density profile as their massive host but with different concentration parameters. These models have been flagged with the following prescriptions:

- *B*-models assume the $c(M)$ relation of B01 for $M > 10^4 M_\odot$;

- *ENS*-models, use the ENS01 model for $M > 10^4 M_\odot$;

- In models flagged as z_0 the low mass extrapolation of the concentration parameter is normalized to that of field haloes of $10^{-6} M_\odot$ measured in the numerical simulation of Diemand et al. 2005 (DMS05) at $z = 26$ and linearly extrapolated at $z = 0$, i.e. $c(10^{-6} M_\odot, z = 0) = c(10^{-6} M_\odot, z = 26) \times (1 + 26)$. The underlying assumption is that, as in the Press-Schechter approach, all existing haloes have just formed, and the $(1 + 26)$ scaling is required to account for the change in the mean density between $z = 26$ and $z = 0$;

- Models flagged as z_c assume instead that, once formed, subhaloes that survive to $z = 0$ do not change their density profile. Therefore for each subhalo of mass M we determine its collapse redshift z_c (defined as in B01 for $M > 10^4 M_\odot$) and compute its concentration parameter accordingly, as $c(M, z = z_c) = c(M, z = 0)/(1 + z_c)$, where $c(M, z = 0)$ is computed as in the z_0 case. The small mass normalization is the same as in models z_0 , rescaled for the smallest masses collapse redshift $z_c(M = 10^{-6} M_\odot) = 70$ suggested by DMS05 and used by Koushiappas 2006. In Fig. 1 we show the collapse redshift as a function of the mass adopted in the z_c -models (thin line);

- Models flagged 5σ assume that all existing subhaloes with mass $M = 10^{-6} M_\odot$ form at the 5σ peaks of the density field, which has the effect of increasing the normalization to $c(10^{-6} M_\odot, z = 0) = 400$;

- Models flagged as *ref*, z_0 and *ref*, z_c are identical to the corresponding z_0 and z_c models for $M > 10^4 M_\odot$. Indeed, they use a naïve extrapolation of the B01 model at low masses, both for the collapse redshift (thick line in Fig. 1) and for the concentration parameter (filled circles in Fig. 2). Though this extrapolation is not supported by numerical simulations, it intuitively reflects the theoretical flatter of the $\sigma(M)$ curve at low masses.

The $c(M)$ profile for each of the z_0 models is shown in Fig.2.

Finally, as pointed out in B01, the $c(M)$ relation is not deterministic. Instead, for a fixed mass, the probability of a given value for $c(M)$ is well described by a lognormal distribution

$$P(c(M)) = \frac{1}{\sqrt{2\pi}\sigma_c \bar{c}(M)} e^{-\left(\frac{\ln(c(M)) - \ln(\bar{c}(M))}{4\sigma_c}\right)^2}, \quad (4)$$

where the mean $\bar{c} = c(M)$ is the concentration parameter of B01 or ENS and the dispersion $\sigma_c = 0.24$ does not depend on the halo mass (B01). In the following, we include this lognormal scatter in all models described in Table 1.

We will not consider in this paper the possibility that subhaloes might contain sub-substructures (Strigari et al. 2007, Diemand 2007a) and that their concentration (and scatter) might depend on the distance from the Galactic Centre (Diemand et al. 2007b). Indeed, such features are found in numerical simulations capable of resolving large sub-haloes ($M > 10^6 M_\odot$) but there is no evidence whether they also apply to much smaller haloes, with masses down to $10^{-6} M_\odot$.

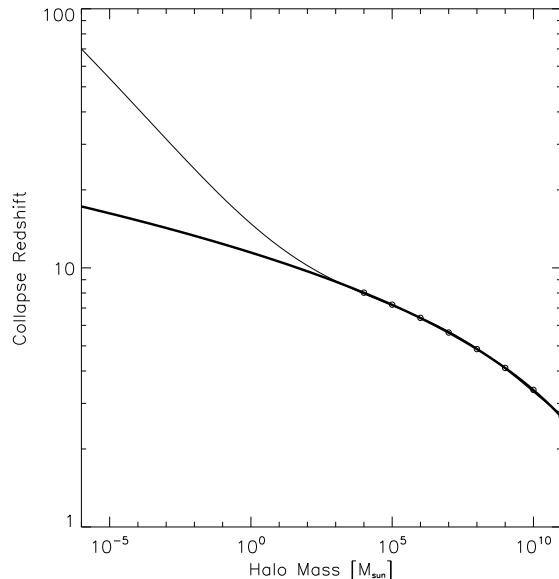


Figure 1. Collapse redshift, z_c , as a function of the halo mass for model B01 (points) for $M > 10^4 M_\odot$. The thin line shows the extrapolation at low masses normalized to the DMS05 value for $z_c(10^{-6} M_\odot)$. The thick line shows a naïve extrapolation of the B01 model at low masses.

3 γ -RAY FLUX FROM ANNIHILATION IN DM CLUMPS

The photon flux from neutralino annihilation in galactic subhaloes, from a direction in the sky making an angle ψ from the Galactic Center (GC), and observed by a detector with angular resolution θ , can be factorized into a term depending only on particle physics parameters, $d\Phi^{\text{PP}}/dE_\gamma$ and a term depending only on cosmological quantities, $\Phi^{\text{cosmo}}(\psi, \theta)$:

$$\frac{d\Phi_\gamma}{dE_\gamma}(E_\gamma, \psi, \theta) = \frac{d\Phi^{\text{PP}}}{dE_\gamma}(E_\gamma) \times \Phi^{\text{cosmo}}(\psi, \theta) \quad (5)$$

3.1 Particle physics contribution

The first factor of Eq.5 can be written as:

$$\frac{d\Phi^{\text{PP}}}{dE_\gamma}(E_\gamma) = \frac{1}{4\pi} \frac{\sigma_{\text{ann}} v}{2m_\chi^2} \cdot \sum_f \frac{dN_\gamma^f}{dE_\gamma} B_f \quad (6)$$

where m_χ denotes the Dark Matter particle mass and dN_γ^f/dE_γ is the differential photon spectrum per annihilation relative to the final state f , with branching ratio B_f . Although the nature of the DM particle is unknown, we can make an educated guess on the physical parameters entering in the above equation. The most commonly discussed DM candidates are the so-called neutralinos, arising in Super-symmetric extensions of the Standard Model of particle physics [SUSY], and the $B^{(1)}$ particles, first excitation of the hypercharge gauge boson in theories with Universal Extra Dimensions [UED] (see Bergström 2000, Bertone et al. 2005b and references therein). Typical values for the mass of these candidates range from ~ 50 GeV up to several TeV. The annihilation cross section can be as

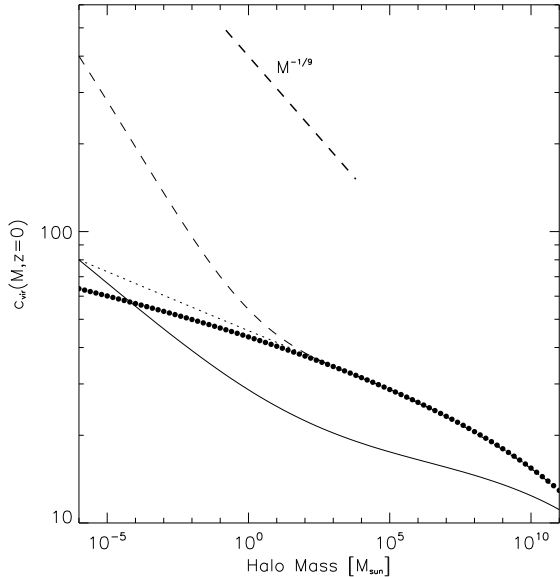


Figure 2. Concentration parameters as a function of halo mass at $z = 0$ computed for the ENS_{z_0} (solid), B_{z_0} (dotted) and the $B_{z_0,5\sigma}$ (dashed) model described in the text. Filled circles show the B01 model naïvely extrapolated at low masses (B_{ref,z_0} model).

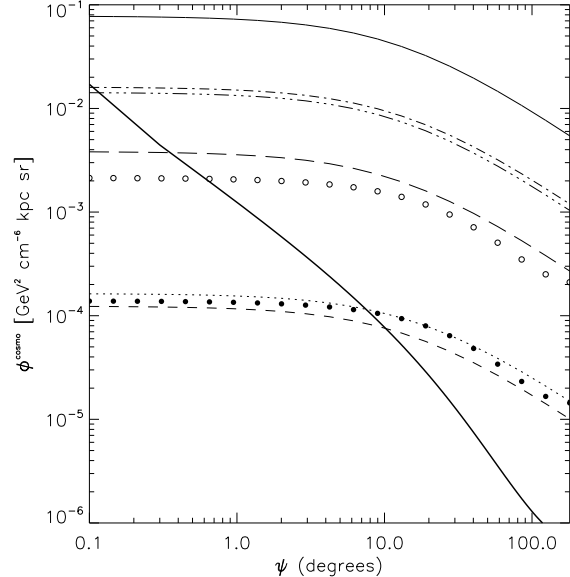


Figure 4. Φ^{cosmo} as a function of the angular distance from the Galactic center, for the MW smooth component (solid thick line) and for unresolved clumps in model $B_{z_c,5\sigma}$ (solid thin line), B_{z_c} (dot-dashed), ENS_{z_c} (long dot-dashed), $B_{z_0,5\sigma}$ (long dashed), B_{ref,z_c} (open circles), B_{z_0} (dotted), B_{ref,z_0} (filled circles) and ENS_{z_0} (dashed). The mass function slope is $\alpha = 1$.

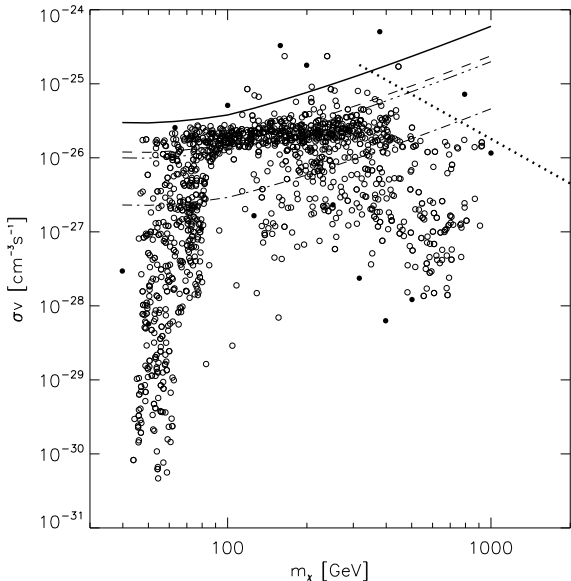


Figure 3. Exclusion plot in the $(\sigma_{\text{ann}}v, m_\chi)$ plane. The solid line corresponds to our best case particle physics scenario, adopted for all the z_0 models. Models above the dashed (long dot-dashed, dot-dashed) curve violate the EGRET extra galactic background (EGB) flux constraints in scenario ENS_{z_c} ($B_{z_c}, B_{z_c,5\sigma}$) for a mass function slope $\alpha = 1$. For comparison, we show with filled (empty) dots a scan of SUSY models with relic density within 2 (5) standard deviations from the WMAP+SDSS value. The dotted line corresponds to the UED model. Supersymmetric models were obtained using the DARKSUSY package (Gondolo et al. , 2004)

high as $\sigma_{\text{ann}}v = 3 \times 10^{-26} \text{cm}^3 \text{s}^{-1}$, as appropriate for thermal relics that satisfy the cosmological constraints on the present abundance of Dark Matter in the Universe. However, we note that the annihilation cross section can be much smaller, as the appropriate relic density can be achieved through processes such as co-annihilations (Bergström 2000, Bertone et al. 2005a). This can be seen from Fig. 3 that shows the range of $\sigma_{\text{ann}}v$ and m_χ allowed in the UED and SUSY models: solid (empty) circles correspond to models with relic density within 2 (5) standard deviations from the WMAP+SDSS suggested value $\Omega_{DM}h^2 = 0.1050^{+0.0041}_{-0.0040}$, where as usual Ω_{DM} is the DM density in units of the critical density, and h is the Hubble parameter in units of $100 \text{km s}^{-1} \text{kpc}^{-1}$, $h = 0.730^{+0.019}_{-0.019}$ (Tegmark et al. 2006).

In order to optimize the prospects for detection, we adopt here a very low value for the particle mass, $m_\chi = 40 \text{GeV}$, together with a high annihilation cross section $\sigma_{\text{ann}}v = 3 \times 10^{-26} \text{cm}^3 \text{s}^{-1}$. As for the nature of the DM particle, we assume here a 100% branching ratio in $b\bar{b}$ and the $dN_\gamma^{b\bar{b}}/dE_\gamma$ functional form of Fornengo et al. 2004. The results can be rescaled for any other candidate, although in most cases the photon spectrum arising from annihilations yields similar results.

3.2 Annihilation flux from diffuse matter and unresolved clumps

The contribution of unresolved substructures to the annihilation signal is given by

$$\Phi^{\text{cosmo}}(\psi, \Delta\Omega) = \int_M dM \int_c dc \int_{\Delta\Omega} \int d\theta d\phi \int_{1.o.s} d\lambda$$

$$[\rho_{sh}(M, R(R_\odot, \lambda, \psi, \theta, \phi)) \times P(c) \times \Phi_{halo}^{\text{cosmo}}(M, c, r(\lambda, \lambda', \psi, \theta', \phi')) \times J(x, y, z|\lambda, \theta, \phi)] \quad (7)$$

where $\Delta\Omega$ is the solid angle of observation pointing in the direction of observation ψ and defined by the angular resolution of the detector θ ; $J(x, y, z|\lambda, \theta, \phi)$ is the Jacobian determinant; R is the galactocentric distance, which, inside the cone, can be written as a function of the line of sight (λ) and the solid angle (θ and ϕ) coordinates and the pointing angle ψ through the relation $R = \sqrt{\lambda^2 + R_\odot^2 - 2\lambda R_\odot C}$, where R_\odot is the distance of the Sun from the Galactic Center and $C = \cos(\theta)\cos(\psi) - \cos(\phi)\sin(\theta)\sin(\psi)$; r is the radial coordinate inside the single subhalo located at distance λ from the observer along the line of sight defined by ψ and contributing to the diffuse emission. The expression

$$\Phi_{halo}^{\text{cosmo}}(M, c, r) = \int \int_{\Delta\Omega} d\phi' d\theta' \int_{1.o.s} d\lambda' \left[\frac{\rho_\chi^2(M, c, r(\lambda, \lambda', \psi, \theta', \phi'))}{\lambda^2} J(x, y, z|\lambda', \theta', \phi') \right]; \quad (8)$$

describes the emission from such a subhalo. Here, $\rho_\chi(M, c, r)$ is the Dark Matter density profile inside the halo.

By numerically integrating Eq. 7, we estimate the contribution to Φ^{cosmo} from unresolved clumps in a 10^{-5} sr solid angle along the direction ψ , for each substructure model considered. The result is shown in Fig. 4. In the same figure, the solid thick line corresponds to the contribution from the MW smooth halo component described in Sec.2.1, which is computed according to Eq.8, with the distance to the observer $\lambda = R_\odot$.

We summarize the properties of the smooth subhalo contribution in Table 2. In the second and third column we show, for each model, the contribution to Φ^{cosmo} in units of $\text{GeV}^2 \text{cm}^{-6} \text{kpc sr}$ towards the Galactic center ($\psi = 0^\circ$) and the angle ψ_d beyond which the smooth subhalo contribution starts dominating over the MW halo foreground. In the fourth column we show the boost factor for each model, computed as the ratio of the integral over the MW volume of the density squared including subhaloes to the same integral for the smooth MW only:

$$b = \frac{\int_{MW} dV (\rho_{MW}^2 + \rho_{sh}^2)}{\int_{MW} dV \rho_{MW}^2} \quad (9)$$

To set the two remaining parameters that determine the intensity of the annihilation flux, namely the particle mass m_χ and the annihilation cross section $\sigma_{\text{ann}}v$ we adopt the most optimistic combination allowed by the SUSY and UED models shown in Fig. 3 that do not exceed the current EGRET upper limits for the annihilation flux above 3 GeV and within a solid angle of 10^{-5} sr. The latter receives contribution from two distinct components: the first one is of Galactic origin, dominates for $\psi < 40^\circ$ and is characterized by a power-law photon spectrum, that leads, upon extrapolation at high energies (Bergström et al. 1998) to the following parametrization

$$\frac{d\phi_{\text{diffuse}}^{\text{gal}-\gamma}}{d\Omega dE} = N_0(l, b) 10^{-6} E_\gamma^{-2.7} \frac{\gamma}{\text{cm}^2 \text{sr GeV}}, \quad (10)$$

where l and b are the galactic latitude and longitude. The normalization factor N_0 depends only on the interstellar

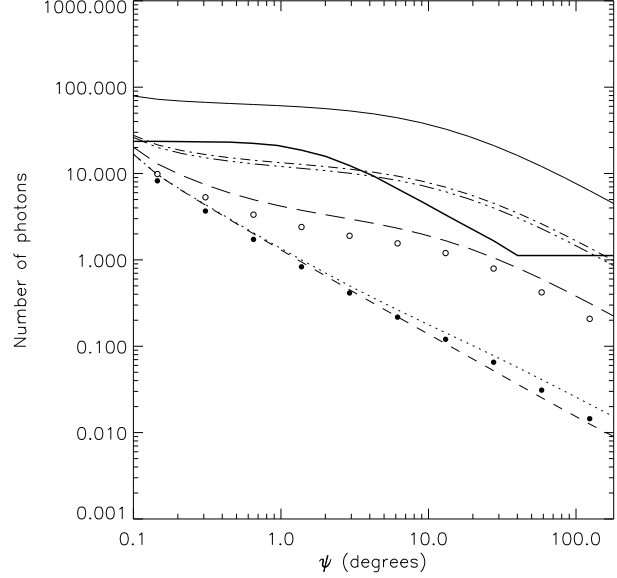


Figure 5. Number of photons above 3 GeV, in 1 year in a solid angle of 10^{-5} sr, as a function of the angle ψ from the GC. From top to bottom, the lines correspond to the $B_{z_c,5\sigma}$, B_{z_c} , ENS_{z_c} , $B_{z_0,5\sigma}$, B_{z_0} and ENS_{z_0} model. Empty (filled) circles show the B_{ref,z_c} (B_{ref,z_0}) model. $\sigma_{\text{ann}}v = 3 \times 10^{-26} \text{cm}^3 \text{s}^{-1}$, $m_\chi = 40 \text{GeV}$ and $BR_{b\bar{b}} = 100\%$ have been used, corresponding to the best value $\Phi_{PP} = 2.6 \times 10^{-9} \text{cm}^4 \text{kpc}^{-1} \text{GeV}^{-2} \text{s}^{-1} \text{sr}^{-1}$. The solid thick line shows the EGRET diffuse expected Galactic and extragalactic background computed along $l = 0$. The mass function slope is $\alpha = 1$.

Results for subhalo models				
Model	Φ_0^{cosmo}	ψ_d	b	Φ_{-9}^{PP}
B_{ref,z_0}	1.4×10^{-4}	7.5	8	2.6
B_{z_0}	2.0×10^{-4}	7.5	10	2.6
$B_{z_0,5\sigma}$	3.6×10^{-3}	0.4	150	2.6
B_{ref,z_c}	2.1×10^{-3}	0.6	120	2.6
B_{z_c}	1.6×10^{-2}	0.1	750	0.9
$B_{z_c,5\sigma}$	7.7×10^{-2}	0.0	3300	0.2
ENS_{z_0}	1.2×10^{-4}	12.0	6	2.6
ENS_{z_c}	1.4×10^{-2}	0.16	660	1.0

Table 2. Results for the halo models. Column 1: Model name. Column 2: Φ_0^{cosmo} [$\text{GeV}^2 \text{cm}^{-6} \text{kpc sr}$] toward the Galactic Center. Column 3: Angle at which the subhalo diffuse contribution dominates over the MW smooth foreground [degrees]. Column 4: boost factors. Column 5: Φ_{-9}^{PP} [$10^{-9} \text{cm}^4 \text{kpc}^{-1} \text{GeV}^{-2} \text{s}^{-1} \text{sr}^{-1}$]. The value for the z_0 and the B_{ref,z_c} models correspond to our best case particle physics scenario. Values for the z_c models except the B_{ref,z_c} are normalized to EGRET data.

matter distribution, and is modeled as in Bergstrom et al. 1998.

The second one is extragalactic, dominates at $\psi > 40^\circ$, and for its photon spectrum we use an extrapolation from low energy EGRET data, following Sreekumar et al. 1998:

$$\frac{d\phi_{\text{diffuse}}^{\text{extra-}\gamma}}{d\Omega dE} = 1.38 \times 10^{-6} E^{-2.1} \frac{\gamma}{\text{cm}^2 \text{ s sr GeV}}. \quad (11)$$

The thick line in Fig. 5 shows the EGRET photon flux as a function of ψ . The EGRET flux is computed according to Eqs. 10 and 11 extrapolated above 3 GeV, within a field of view of 10^{-5} sr in 1 year of observation. The flux is computed along $l = 0$, that is away from the Galactic plane, where the EGRET flux is minimum. The Galactic and extragalactic contributions are clearly visible. The other curves show the predictions for all models in Table 1, obtained when using our best case particle physics scenario described in Sec. 3.1 that corresponds to $\Phi^{PP} = 2.6 \times 10^{-9} \text{ cm}^4 \text{ kpc}^{-1} \text{ GeV}^{-2} \text{ s}^{-1} \text{ sr}^{-1}$. All the values of $\sigma_{\text{ann}}v$ and m_χ that would result in the same Φ^{PP} are represented with a solid line in Fig.3.

With this choice of parameters all models flagged with z_c (but the B_{ref,z_c}), for which the halo properties are computed at the collapse redshift, exceed experimental data close to the GC and for $\psi > 40^\circ$, where the EGRET flux is assumed to have an extragalactic origin. We do not regard the mismatch at small angles as significant, because of the limited angular resolution of the original EGRET data. On the contrary, we decrease the values of Φ^{PP} to bring the z_c -models into agreement with data at large angles from the GC. The values of Φ^{PP} adopted in each model are listed in the last column of Table 2. We note that a smaller Φ^{PP} corresponds to assuming a larger particle mass or a smaller cross section. The $[\sigma_{\text{ann}}v, m_\chi]$ phase space parameter allowed for SUSY (circles) or UED (dotted line) models is shown in Fig. 3. In the same figure the three dashed and dot-dashed lines correspond to the EGRET constrained values of Φ^{PP} for the z_c models. The particle physics models above the corresponding line are thus excluded by EGRET data.

3.3 Annihilation flux from individual clumps

Besides the diffuse signal produced by annihilation in both the subhalo population and the smooth MW component, we consider here the contribution from individual subhaloes, that we regard as Poisson fluctuation of the underlying mean distribution of subgalactic haloes that could be detected as isolated structures. To estimate their flux we consider 10 independent Monte Carlo realizations of the closest and brightest subhaloes, in a cone of $\sim 50^\circ$ pointing toward the Galactic Center. To do this we generate, for each mass decade, the positions of those subhaloes that have $\Phi^{\text{cosmo}} > \langle \Phi_{B_{z_0}}^{\text{cosmo}}(\psi = 50^\circ) \rangle \sim 5 \times 10^{-5} \text{ GeV}^2 \text{ cm}^{-6} \text{ kpc sr}$, where the brackets indicate the mean annihilation flux. If $N < 100$ such objects are found, then we still include the remaining $100 - N$ nearest subhaloes in that mass range.

Adding contribution from an increasing number of individual haloes monotonically increases the chance of subhalo detection within the angular resolution element of the detector. To check whether our procedure is robust and the number of detectable haloes has converged we reduced the

number of Monte Carlo-generated haloes by 70 % and found that probability of subhalo detection indeed remains constant.

To summarize, for each model, the total contribution to Φ^{cosmo} is given by the sum of three terms: the diffuse contribution coming from unresolved haloes, corresponding to the mean contribution of the clumpy component computed with Eq.7, the contribution of the diffuse smooth Galactic component and that of individual nearby subhaloes, both computed using Eq.8. Figs.6 and 7 show the three contributions to Φ^{cosmo} for the models B_{ref,z_c} and ENS_{z_0} , respectively. In each figure, the contribution from unresolved clumps is shown in the upper left panel, the one from the diffuse MW in the upper right, the one from resolved clumps in the lower left, and the sum of all contributions in the lower right panel. The smooth MW halo contribution falls rapidly with the distance from the GC, while the diffuse subhalo contribution keeps a high value even at large angular distances. The single halo contribution is almost completely hidden by the overwhelming diffuse foreground, while it is nicely resolved as a standalone component.

The same procedure described in this section for a cone pointing to the GC has been repeated for two other regions: a cone pointing to the Galactic anticenter and a cone to the Galactic pole $b = 90^\circ$. The purpose is to compute the annihilation flux and to evaluate the number of detectable subhalos over the whole sky.

4 PROSPECTS FOR DETECTION

In absence of strong features in the annihilation spectrum, the best chances to detect the annihilation signal within our Galaxy is to observe some excess on the γ -ray sky either due to diffuse emission or to resolved sources that have no astrophysical counterpart. However, the requirements for signal detection are different in the two cases since the smooth annihilation flux, that contributes to the signal in the first case, adds to the noise in the second.

To determine the probability of halo detection, we consider a 1 year effective exposure time performed with a GLAST-like satellite. We note that, given the 2.4 sr field of view and the all-sky survey mode of GLAST, such an exposure will be achieved in about 5 years of actual observation time.

The prospects for detecting γ -rays from DM annihilations are evaluated by comparing the number n_γ of expected signal photons to the fluctuations of background events n_{bkg} . To this purpose we define the sensitivity σ as:

$$\begin{aligned} \sigma &\equiv \frac{n_\gamma}{\sqrt{n_{\text{bkg}}}} \\ &= \sqrt{T_\delta} \epsilon_{\Delta\Omega} \frac{\int A_\gamma^{\text{eff}}(E, \theta_i) [d\phi_\gamma^{\text{signal}}/dE d\Omega] dE d\Omega}{\sqrt{\int \sum_{\text{bkg}} A_{\text{bkg}}^{\text{eff}}(E, \theta_i) [d\phi_{\text{bkg}}/dE d\Omega] dE d\Omega}} \end{aligned} \quad (12)$$

where T_δ defines the effective observation time and ϕ_{bkg} is the background flux. The quantity $\epsilon_{\Delta\Omega}$ is the fraction of signal events within the optimal solid angle $\Delta\Omega$ corresponding to the angular resolution of the instrument and is usually ~ 0.7 . We set it equal to 1 to get the most optimistic values. The effective detection area A^{eff} for electromagnetic or

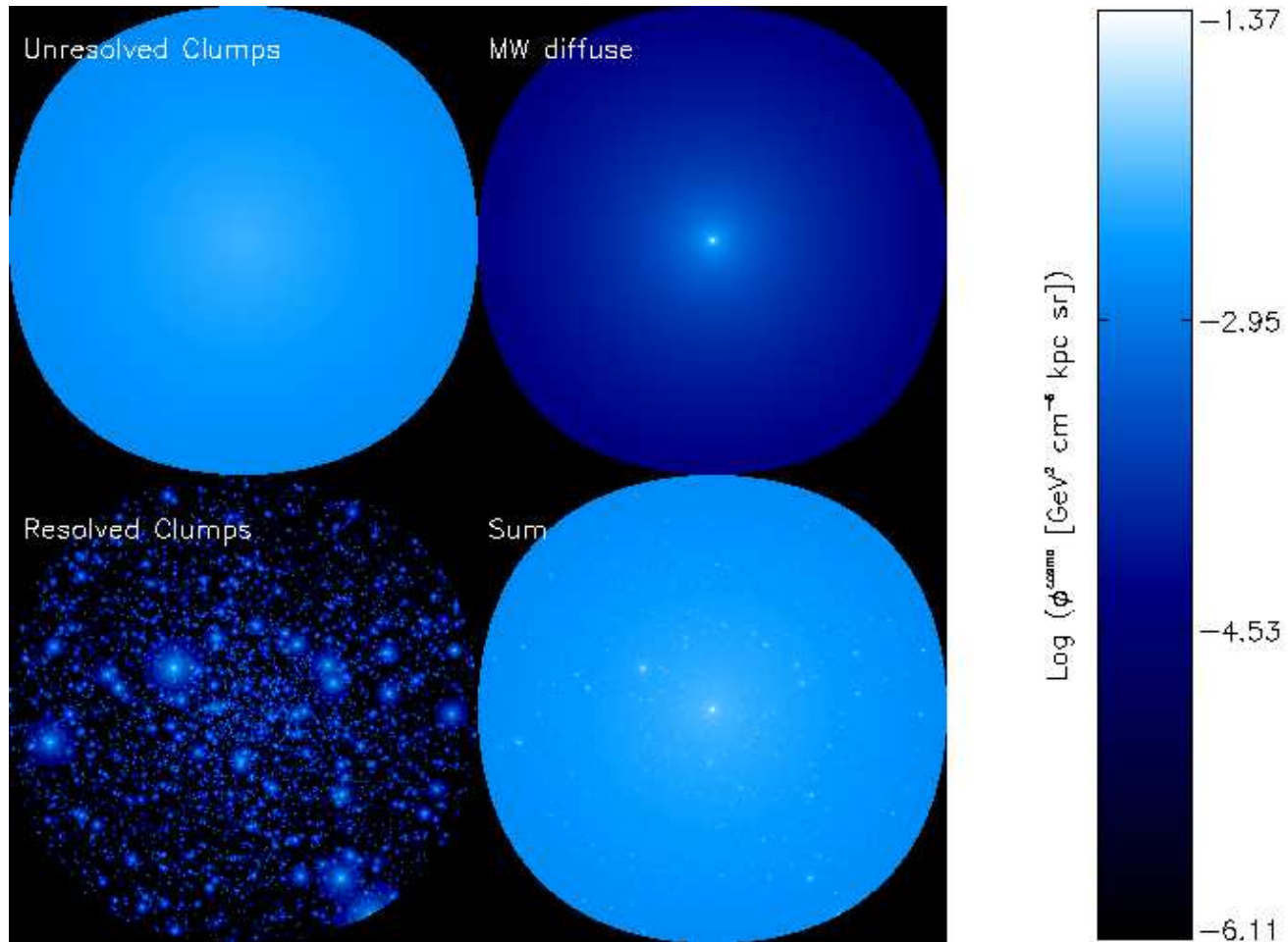


Figure 6. Map of Φ^{cosmo} (proportional to the annihilation signal) for the $B_{ref,zc}$ model, in a cone of 50° around the Galactic Center, as seen from the position of the Sun. Upper left: smooth subhalo contribution from unresolved haloes. Upper right: MW smooth contribution. Lower left: contribution from resolved haloes. Lower right: sum of the three contributions.

hadronic particles is defined as the detection efficiency times the geometrical detection area. In the following we make the realistic assumption that all hadronic particles will be identified, so that the background will be composed by photons only. We also assume that all photons will be correctly identified, which is somehow optimistic, since there will be a small amount (a few percent) of irreducible background due, e.g., to the backscplash of high energy photons.

We use $A^{\text{eff}} = 10^4 \text{ cm}^2$, independent from the energy E and the incidence angle θ_i , and an angular resolution of 0.1° . Both these values are rather optimistic, since the expected GLAST angular resolution approaches 0.1° only at about 20 GeV, while the on-axis effective area is quoted to be maximum $\sim 8 \times 10^3 \text{ cm}^2$ above 1 GeV and decreases by $\sim 20\%$ for an incidence angle of 20° .

As anticipated, different annihilation signals need to be compared with different background noises. For the detection of the diffuse annihilation flux the background is contributed both by Galactic (Eq. 10) and extragalactic astrophysical sources (Eq. 11) measured by EGRET. In the case of individual subhaloes, the annihilation photons produced in the smooth Galactic halo and in the unresolved clumpy component contribute to the background rather than to the signal.

4.1 Sensitivity to diffuse emission

We first study the sensitivity σ of such a GLAST-like observatory to the annihilation flux from the smooth DM profile and from the diffuse contribution of unresolved subhaloes. Both signals are computed above 3 GeV, and the astrophysical background noise is obtained from Eqs.10 and 11 specified along $l = 0$.

The result is shown in Fig.8, where we plot the statistical significance of the detection as a function of ψ for each of the models listed in Table 2.2. 1σ detections of the annihilation signal is expected at $\psi < 40^\circ$ for all the models labelled zc . The chances of observing the diffuse annihilation flux are significantly higher in the direction of the Galactic Center along which models labelled $z0$ predict a signal detectability as high as 5σ . Yet, these predictions should be taken with much care since the measured astrophysical γ -ray flux above 3 GeV in the direction of the GC, which constitutes the background, is known with large uncertainties.

4.2 Detection of individual haloes

Subhaloes can also be detected through the annihilation flux produced by individual, nearby clumps that would appear as

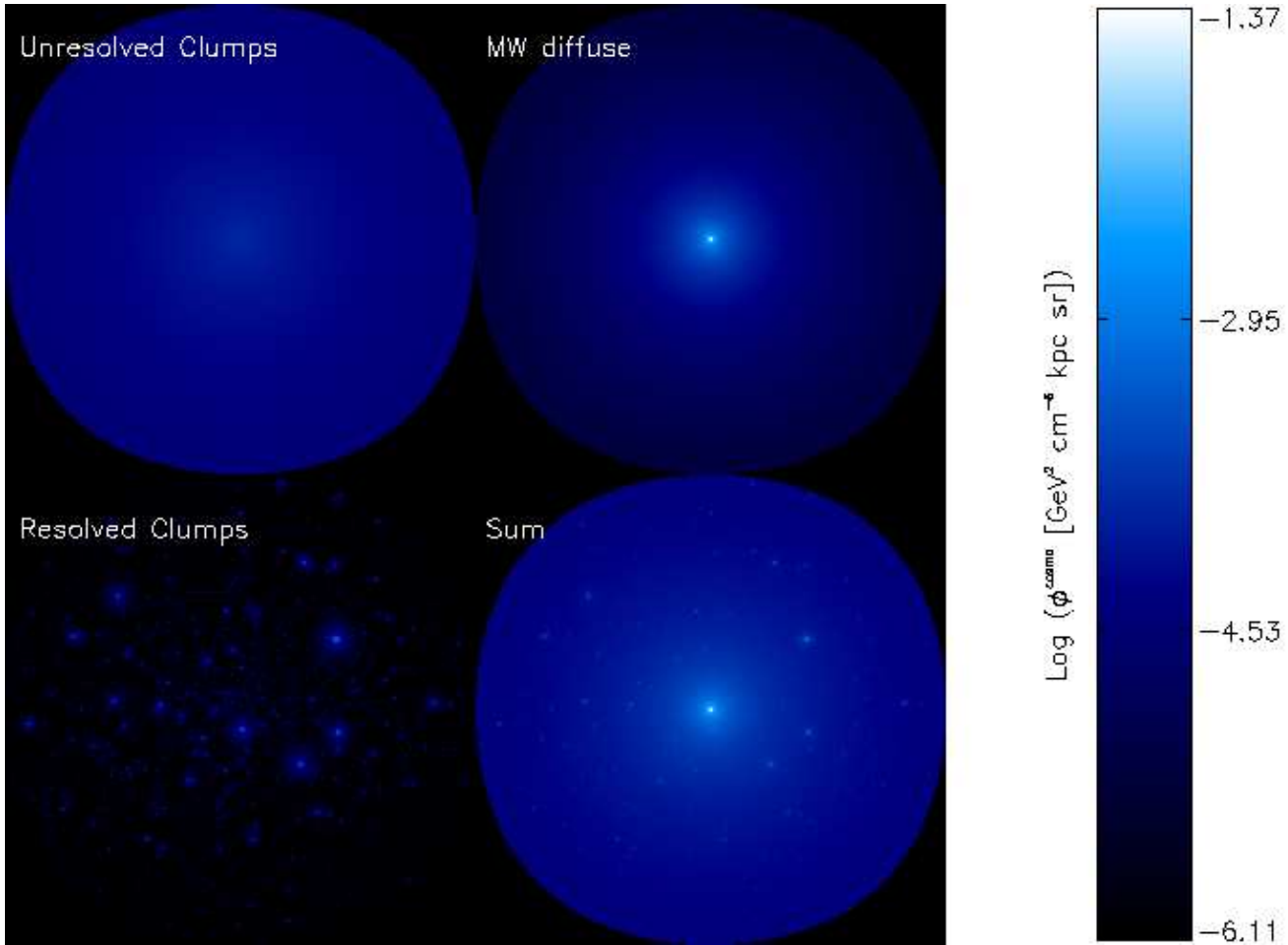


Figure 7. Same as in Fig. 6 for the ENS_{z_0} model.

bright, possibly extended, sources, as shown in the bottom right panels of Figs. 6 and 7. In this case the signal is produced within the individual haloes of our Monte Carlo realizations, while the background is contributed by the smooth astrophysical background plus the diffuse annihilation flux produced by the Galaxy and its subhaloes. For each halo in the 10 Monte Carlo realizations, and for each virial concentration model, we

- assign to it an arbitrary concentration parameter $c(M)$;
- calculate the annihilation signal;
- find the value of the concentration parameter that guarantees a 5σ detection in 1 year exposure time, $c_{5\sigma}(M)$;
- identify the probability of detection of the clump with the probability $P(> c_{5\sigma})$ that such a clump has a concentration as high as $c_{5\sigma}(M)$, assuming the lognormal distribution described in Eq.4.

The total number of detectable subhaloes is then simply given by $\sum_i P_i(> c_{5\sigma})$, where the sum is performed over all haloes in the realization. Results are obtained by averaging over all over the 10 Monte Carlo realizations and the procedure is repeated for all models listed in Table 1.

The number of haloes that can be detected in 1 year with a significance above 5σ in cone of view with angular opening of 50° towards the GC is shown in Fig.9 for the z_0

models and in Fig. 10 for the zc models, as a function of the subhaloes mass. Had we assumed a deterministic relation for $c(M)$ the number of events would have decreased by a factor ~ 2 .

At higher latitudes the number of haloes indeed reduces, but this is compensated by the lower foreground given by the smooth subhalo component. The maximum number of detectable events is obtained toward $b = 90$ where these two effects interplay in a most favourable way for the detection.

Table 3 lists the number of haloes that can be detected with a significance larger than 5σ in a cone of 50° around the Galactic Center (first column), the Galactic pole (second column) and the Galactic anticenter (third column), for each model, for our reference mass function slope $\alpha = 1$ and the Φ_{PP} values listed in Table 2. Hereafter, each error is the standard deviation obtained averaging over the 10 MC representations. The effect of decreasing the number of haloes far from the GC is compensated by the lower foreground due to the diffuse subhalo contribution to the annihilation flux. The best compromise is found around the Galactic poles.

In Table 4 we show the total number of haloes that can be detected with a GLAST-like satellite in the whole sky with a significance larger than 5σ , with a mass function slope $\alpha = 1$ (first column) and Φ_{PP} values listed in Table 2.

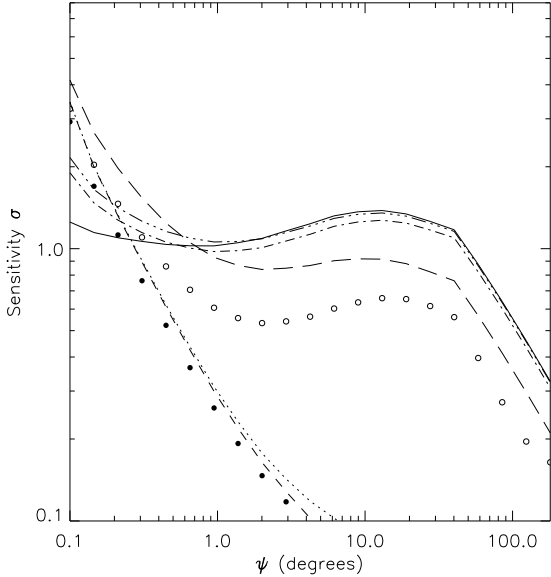


Figure 8. Statistical significance, as a function of the angle from the GC ψ , for the detection of the DM annihilation flux from diffuse subhaloes plus the MW smooth component (along $l = 0$), for the different models explored: B_{z_0} (dotted line), ENS_{z_0} (short dashed), B_{ref,z_0} (filled circles), B_{ref,z_c} (empty circles), $B_{z_0,5\sigma}$ (long dashed), B_{z_c} (long dot-dashed), ENS_{z_c} (dot-dashed), $B_{z_c,5\sigma}$ (solid). The mass function slope is $\alpha = 1$. We refer to Table 2 for the values of Φ_{PP} used in this figure.

Model	Number of detectable haloes ($\alpha = 1$)		
	$N_{GC}^{5\sigma}$	$N_{90}^{5\sigma}$	$N_{180}^{5\sigma}$
B_{ref,z_0}	0.65 ± 0.45	0.85 ± 0.43	0.59 ± 0.30
B_{z_0}	0.65 ± 0.45	0.84 ± 0.43	0.59 ± 0.30
$B_{z_0,5\sigma}$	0.46 ± 0.34	0.60 ± 0.34	0.50 ± 0.27
B_{ref,z_c}	16.16 ± 2.60	23.24 ± 2.28	18.55 ± 1.72
B_{z_c}	1.74 ± 0.92	2.40 ± 0.82	2.15 ± 0.65
$B_{z_c,5\sigma}$	0.05 ± 0.05	0.07 ± 0.08	0.08 ± 0.08
ENS_{z_0}	0.06 ± 0.12	0.07 ± 0.10	0.04 ± 0.07
ENS_{z_c}	0.29 ± 0.40	0.49 ± 0.37	0.46 ± 0.30

Table 3. Number of haloes detectable, at 5σ in 1 year of effective observation with a GLAST-like satellite, in a 50° f.o.v. cone towards the GC (column 1), the Galactic pole (column 2) and the anticenter (column 3). The subhaloes mass function slope is $\alpha = 1$. We refer to Table 2 for the values of Φ_{PP} used in this table.

The remaining two columns show the effect of adopting a mass function with power-law index $\alpha = 0.95$ (second column) and $\alpha = 0.9$ (third column). Adopting a shallower mass function increases in most cases the number of detectable subhalos. However, the magnitude of the effect, that results from the lowering of the unresolved background,

Model	Total number of detectable haloes		
	$N_{tot}^{5\sigma} (\alpha = 1)$	$N_{tot}^{5\sigma} (\alpha = 0.95)$	$N_{tot}^{5\sigma} (\alpha = 0.9)$
B_{ref,z_0}	4.30 ± 4.00	3.62 ± 3.30	3.51 ± 2.11
B_{z_0}	4.26 ± 3.97	3.61 ± 3.30	3.50 ± 2.13
$B_{z_0,5\sigma}$	3.12 ± 3.09	3.30 ± 3.17	3.43 ± 2.04
B_{ref,z_c}	118.36 ± 24.96	132.89 ± 30.15	125.03 ± 20.06
B_{z_c}	12.53 ± 8.67	104.23 ± 24.78	119.04 ± 19.77
$B_{z_c,5\sigma}$	0.39 ± 0.56	10.55 ± 6.36	96.34 ± 18.66
ENS_{z_0}	0.33 ± 0.89	0.67 ± 1.58	0.34 ± 0.50
ENS_{z_c}	2.50 ± 4.48	23.43 ± 10.17	30.40 ± 10.31

Table 4. Total number of haloes detectable over the whole sky, at 5σ in 1 year of effective observation with a GLAST-like satellite, for a mass function slope $\alpha = 1$ (column 1), $\alpha = 0.95$ (column 2) and $\alpha = 0.9$ (column 3). We refer to Table 2 for the values of Φ_{PP} used in this table.

whose main contribution is given by small sub-haloes, depends on the model explored.

As expected, we can observe how this effect is larger for those models whose overall contribution to Φ^{cosmo} is larger, that is for those models whose concentration parameters have been computed at the collapse redshift. The effect is reduced for the other models, as well as for the B_{ref,z_c} one, for the following reason: when using $\alpha = 1$, the Φ^{PP} value for the z_c models (but the B_{ref,z_c} one) has been decreased in order to respect the EGRET EGB limit, while when using $\alpha = 0.9$ all models fulfill the EGRET EGB constraint, and we can use our best case Φ_{PP} . This is also true for $\alpha = 0.95$, except for the $B_{z_c,5\sigma}$ model, where we have to use $\Phi^{PP} = 0.84 \text{ cm}^4 \text{ kpc}^{-1} \text{ GeV}^{-2} \text{ s}^{-1} \text{ sr}^{-1}$. In fact, the z_0 and the B_{ref,z_c} model experience just a minor increase (compatible within the error bars) of the number of detectable halos; the B_{z_c} and ENS_{z_c} models reach this stability for $\alpha \leq 0.95$, as soon as their Φ^{PP} allowed value gets our best value; the $B_{z_c,5\sigma}$ model keeps on showing a large effect when changing mass function slope, because it is allowed to have the best value Φ^{PP} only when $\alpha = 0.9$.

In the most optimistic B_{ref,z_c} model, we expect that a GLAST-like experiment could detect $\sim 120 - 130$ subhaloes with masses above $10^5 M_\odot$ over all sky, for all the mass function slopes considered in this analysis. In all the models whose concentration parameters are computed at $z = 0$ the number of detectable events is compatible with zero within the errors, whatever slope is used. Accordingly to the aforementioned discussion, the effect of changing the mass function slope is dramatic in the $B_{z_c}(B_{z_c,5\sigma})$ model, for which the total number of events ranges from ~ 10 (~ 0) for $\alpha = 1$ to ~ 120 (~ 100) for $\alpha = 0.9$. A large effect (~ 0 to ~ 30) is observed in the ENS_{z_c} model too.

5 DISCUSSION AND CONCLUSIONS

The prospects for detecting γ -rays from the annihilation of DM particles in substructures of the MW have been inves-

tigated by a number of authors (e.g. Stoehr et al. 2003, Pieri & Branchini 2004, Koushiappas et al. 2004, Oda et al. 2005, Pieri et al. 2005). In this work we confirm that substructures can provide a significant contribution to the expected Galactic annihilation signal, although the actual enhancement depends on the assumptions made on the clump properties, which are affected by large uncertainties. Indeed, given the assumed substructure mass function $dN/dM \propto M^{-2}$, the contribution to the total γ -ray flux by subhaloes of different masses depends on the annihilation signal produced within each clump which is dictated by the internal structure. Numerical experiments have shown that the total annihilation signal is dominated by the highest mass subhaloes both in a Galactic halo at $z=0$ (Stoehr et al. 2003) and in $0.1 M_\odot$ halo host at $z=75$ (Diemand et al. 2006). However, the recent results of the high resolution 'Via Lactea' simulation (Diemand et al 2007a) indicate that the annihilation luminosity is approximately constant per decade of substructure mass while analytical calculations (Colafrancesco et al. 2006) tend to find that the signal is dominated by small mass subhaloes. Indeed this is also the case with our model predictions. Fig. 11 shows the expected contribution of the unresolved haloes to the total annihilation flux as a function of the subhalo mass, integrated on each mass decade. In all the models explored the annihilation signal is dominated by the smallest clumps, as a result of the decrease of the virial concentration with the subhalo mass, as shown in Fig. 2. Under optimistic assumptions on the particle physics parameters of DM particles, a GLAST-like experiment might detect such a DM annihilation flux, but only in a few pixels around the Galactic Center.

It should be noticed, however, that estimates of the annihilation signal from the Galactic Center are affected by the poor knowledge of the DM profile in the innermost regions of the Galaxy, which is usually obtained by extrapolating over many orders of magnitude the results of numerical simulations. The presence of a Supermassive Black Hole at the center of the Galaxy makes things even more complicated, as it may significantly affect the distribution of DM within its radius of gravitational influence, leading to the formation of an overdensity called "spike" (Gondolo and Silk, 1999). Spikes require however rather fine-tuned conditions to form (Ullio et al. 2002) and any overdensity is in any case severely suppressed by the interaction with stars and DM self-annihilations (Merritt et al. 2002, Bertone & Merritt 2005).

In alternative, one could look for an annihilation signal from individual DM substructures, such as dwarf galaxies or even smaller, 'baryon-less', clumps. We have shown that, depending on the assumptions made on the properties of clumps, only large haloes with $M > 10^5 M_\odot$ can be detected and identified with a GLAST-like experiment, which is consistent with the analyses of Stoehr et al. 2003 and Koushiappas et al. 2004. The number of detectable haloes ranges from 0 to more than a hundred, depending on the model. Adopting a shallower subhalo mass function increases the number of detectable subhaloes in those models in which the diffuse annihilation signal is dominated by the unresolved, low mass haloes.

In any case, scenarios leading to a large number of detectable small-scale clumps appear to be severely constrained by the γ -ray background measured by EGRET.

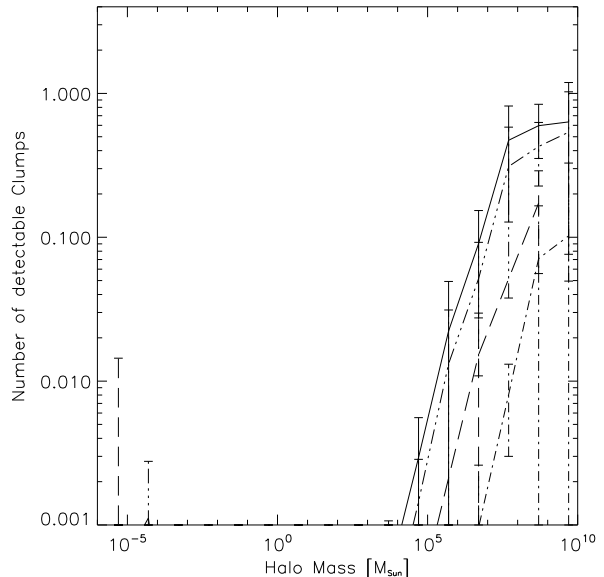


Figure 9. Number of events detectable in 1 year a 5σ with a GLAST-like experiment in a 50 degrees cone towards the GC for the models ENS_{z_0} (dot-dashed), B_{z_0} (solid), $B_{z_0,5\sigma}$ (dashed) and B_{ref,z_0} (long dot-dashed), assuming the lognormal distribution for the concentration parameter. We refer to Table 2 for the used values of Φ_{PP} . The mass function slope is $\alpha = 1$.

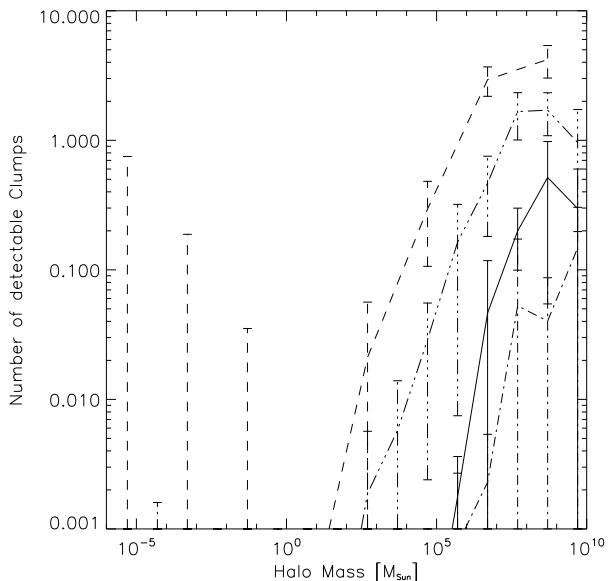


Figure 10. Number of events detectable in 1 year a 5σ with a GLAST-like experiment in a 50 degrees cone towards the GC for the models B_{ref,z_c} (dashed), ENS_{z_c} (solid), B_{z_c} (long dot-dashed) and $B_{z_c,5\sigma}$ (dot-dashed), assuming the lognormal distribution for the concentration parameter. We refer to Table 2 for the used values of Φ_{PP} . The mass function slope is $\alpha = 1$.

In particular, the model of Koushiappas 2006 is similar to our B_{z_c} model, as far the cosmological term is considered, while the particle physics contribution corresponds to our best case scenario $\Phi_{B_{z_0}}^{PP}$. Although nearby haloes would be bright, and observable, in this case, we have shown that the associated diffuse emission produced by all the remaining, unresolved, clumps in the Milky Way, would far exceed the γ -ray background measured by EGRET. The chances to detect the proper motion of clumps are thus very low, as the lowest mass detectable subhaloes, ($M=10^5 M_\odot$), are typically found at a distance greater than 0.5 kpc, leading to a proper motion less than $\sim 0.1' \text{ yr}^{-1}$, well below the GLAST angular resolution of a few arcminutes.

We have made use of simplified and extreme scenarios for the subhaloes concentration parameter models. More accurate scenarios, though not supported by numerical simulations for small mass haloes, could lead to different diffuse foreground levels and to both more or fewer detectable haloes.

One may wonder why we preferentially expect to individually detect the more massive subhaloes, while the unresolved annihilation signal is mainly contributed by small mass clumps. The reason is that the volume over which individual haloes can be detected decreases rapidly with the halo mass. To see this, let us consider the maximum distance D_{MAX} at which a clump can be detected. This distance depends on the halo luminosity which, in turns, depends on the halo mass and concentration. For a NFW profile: $D_{\text{MAX}} \propto M^{0.5} c(M)^{1.5}$. On the other hand, as discussed e.g. by Koushiappas 2006, given a subhalo mass function $dN/dM \propto M^{-2}$, the number of detectable haloes per mass decade is: $dN/d\text{Log}(M) \propto D_{\text{MAX}}^3 M^{-1} \propto M^{0.5} c(M)^{4.5}$. Assuming a simple scale-free virial concentration $c(M) \propto M^{-\gamma}$, we see that if $\gamma > \gamma_{th} = -1/9$, then the number of detectable haloes per mass decade halo indeed increases with the subhalo mass. The $c(M)$ relation for some of our models is shown in Fig. 2 along with the $\gamma_{th} = -1/9$ reference slope (thick dashed line). Models B_{z_0} and ENS_{z_0} , that have $\gamma > \gamma_{th}$ do indeed predict that the probability of subhalo detection increases with the mass (see Fig. 9). On the other hand, the slope of the $c(M)$ relation for $M < 10^2 M_\odot$ is slightly steeper than γ_{th} . Therefore we expect a bimodal probability that peaks at high masses with a secondary maximum for the smallest subhaloes. Indeed, this is what we observe in Figure 9.

In conclusion, we have studied the prospects for indirect detection of Dark Matter in MW subhaloes with a GLAST-like satellite. We have chosen 8 different models for the concentration parameter, which span the phase space the theoretical uncertainties on the Dark Matter halo properties, as well as 3 different values for the subhaloes mass function slope. For each model, we have computed the diffuse emission from unresolved subhaloes, as well as the γ -ray flux from individual, nearby haloes.

We found that for models with concentration parameter computed at $z = 0$ the detection of individual haloes appears challenging, while the diffuse emission from unresolved clumps dominates the MW smooth emission for sky directions > 1 degree off the GC.

In the case of $\alpha = 1$, in all the z_c models except the B_{ref,z_c} , the diffuse emission from unresolved clumps exceeds the EGRET constraints in a portion of the DM param-

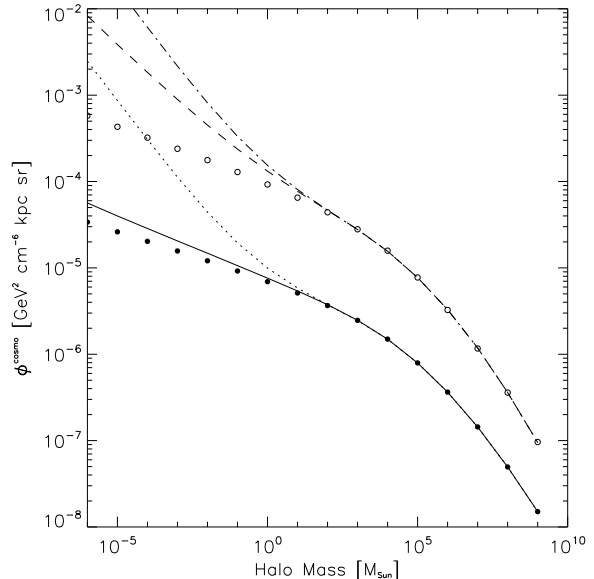


Figure 11. Contribution to Φ_{cosmo} from substructures of mass M integrated over the mass decade, for the different B models explored and computed toward the Galactic Center. Solid and empty circles correspond to the B_{ref,z_0} and B_{ref,z_c} models respectively. Lines show the $B_{z_c,5\sigma}$ (dot-dashed), B_{z_c} (dashed), $B_{z_0,5\sigma}$ (dotted) and B_{z_0} (solid) models. The mass function slope is $\alpha = 1$.

ter space relevant for SUSY models, as shown in Fig. 3. Adopting DM models compatible with the EGRET data, one may still hope to detect individual haloes, like e.g. in the B_{z_c} model.

The B_{ref,z_c} is our best case model for all the values of the mass function slope, though it should be stressed that it is not supported by numerical experiments but only by theoretical considerations. The success of the B_{ref,z_c} model is due to the fact that the diffuse emission expected from subhaloes is dominated by small mass haloes while the large mass haloes are most favourably detected as spare sources. A functional form for the concentration parameter which flattens at low masses, as it is the B_{ref,z_c} one, will in fact decrease the diffuse emission, thus allowing a larger value for Φ_{PP} and consequently increasing the chances of detection for large mass haloes.

In general, adopting the most optimistic set of parameters for the DM particle compatible with EGRET (see Table 2), the number of detectable subhaloes over all sky (at 5σ , with a GLAST-like experiment and a 1-year exposure time), for the 8×3 models we have studied, ranges between 0 and 120.

Yet, it should be noticed that the numbers listed in Table 2 are obtained with a very optimistic value for the Particle Physics involved in the process. If we assume a more realistic model for the Dark Matter particle ($m_\chi = 100 \text{ GeV}$, $\sigma v = 10^{-26} \text{ cm}^3 \text{ s}^{-1}$) instead, we find that at most only a handful of detectable haloes are found (at most a handful over all sky for the most optimistic B_{ref,z_c} model).

In all the models explored, small mass subhaloes are always below the threshold for detection, and their presence could be revealed only through the enhancement of the dif-

fuse foreground emission. The different predicted ratio between diffuse emission and number of detected haloes for the models we have considered, would provide precious information on the underlying cosmology, in case of positive detection.

6 ACKNOWLEDGMENTS

We are indebted to J. Bullock for help and discussion. We thank J. Diemand, S. Koushiappas and G. Tormen for useful discussions, comments and suggestions.

REFERENCES

- Ando S., Komatsu E., 2006, *Phys. Rev. D*, 73, 3521
- Baltz E. A. et al., 2000, *Phys. Rev. D*, 61, 023514
- Baltz E. A., Battaglia M., Peskin M. E., Wizansky T., 2006a, *Phys. Rev. D*, 74, 103521
- Baltz E. A., Taylor J. E., Wai L. L., 2006b, *astro-ph/0610731*
- Berezinsky V. R. et al., 1992, *Phys. Lett. B*, 294, 221
- Bergström L., Ullio P., 1997, *Nucl. Phys. B*, 504, 27
- Bergström L. et al., 1998, *Astropart. Phys.*, 9, 137
- Bergström L., 2000, *Rept. Prog. Phys.*, 63, 793
- Bergström L., Edsjö J., Ullio P., 2001, *Phys. Rev. Lett.*, 87, 25
- Bergström L., Bringmann T., Eriksson M., Gustafsson M., 2005a, *JCAP*, 0504, 004
- Bergström L., Bringmann T., Eriksson M., Gustafsson M., 2005b, *Phys. Rev. Lett.*, 94, 131301
- Bergström L., Bringmann T., Eriksson M., Gustafsson M., 2005c, *Phys. Rev. Lett.*, 95, 241301
- Bergström L., Hooper D., 2006, *Phys. Rev. D*, 73, 063510
- Bertone G., Hooper D., Silk J., 2005a, *Phys. Rept.*, 405, 279
- Bertone G., Zentner A. R., Silk J., 2005b, *Phys. Rev. D*, 72, 103517
- Bertone G., Merritt D., 2005, *Phys. Rev. D*, 72, 103502
- Bertone G., 2006, *Phys. Rev. D*, 73, 103519
- Brun P. et al., *astro-ph/0704.2543*
- Bullock J. et al., 2001, *MNRAS*, 321, 559 (B01)
- Calcaño-Roldan C., Moore B., 2000, *Phys. Rev. D*, 62, 123005.
- Colafrancesco S., Profumo S., Ullio P., 2006, *Astronomy & Astrophysics*, 455, 21
- Diemand J., Moore B., Stadel J., 2004, *MNRAS*, 352, 535
- Diemand J., Moore B., Stadel J., 2005, *Nature*, 433, 389 (DMS05)
- Diemand J., Kuhlen M., Madau P., 2006, *Astrophys. J.*, 649, 1
- Diemand J., Kuhlen M., Madau P., 2007a, *Astrophys. J.*, 657, 262
- Diemand J., Kuhlen M., Madau P., 2007b, *astro-ph/0703337*
- Eke V. R., Navarro J. F., Steinmetz M., 2001, *Astrophys. J.*, 554, 114 (ENS01)
- Evans N. W., Ferrer F., Sarkar S., 2004, *Phys. Rev. D*, 69, 123501
- Fornasa M., Taoso M., Bertone G., *astro-ph/0703757*
- Fornengo N., Pieri L., Scopel S., *Phys. Rev. D*, 70, 103529
- Gao L. et al., 2005, *MNRAS*, 363, 379
- Gondolo P., Silk J., 1999, *Phys. Rev. Lett.*, 83, 1719
- Gondolo P., et al., 2004, *JCAP*, 0407, 008
- Gounaris G. J., Layssac J., Porfyriadis P. I., Renard F. M., 2004, *Phys. Rev. D*, 69, 075007
- Green A. et al., 2004, *MNRAS*, 353, L23
- Green, A. M., Hofmann, S., & Schwarz, D. J. 2005, *JCAP*, 8, 3
- Horiuchi S., Ando S., 2006, *Phys. Rev. D*, 74, 103504
- Jenkins A. et al., 2001, *MNRAS*, 321, 372
- Kazantzidis S. et al., 2004, *ApJ*, 608, 663
- Koushiappas S. M., Zentner A. R., Walker T. P., 2004, *Phys. Rev. D*, 69, 043501
- Koushiappas S. M., 2006, *Phys. Rev. Lett.*, 97, 191301
- Merritt D. et al., 2002, *Phys. Rev. Lett.*, 88, 191301
- Moore B. et al., 2001, *Phys. Rev. D*, 64, 063508
- Muñoz C., 2004, *Int. J. Mod. Phys. A*, 19, 3093
- Navarro J. F., Frenk C. S., White S. D., 1996, *Astrophys. J.*, 462, 563 (NFW)
- Nojiri M. M., Polesello G., Tovey D. R., 2006, *JHEP* 0603, 063
- Oda T., Totani T., Nagashima M., 2005, *Astrophys. J.*, 633, L65
- Pieri L., Branchini E., 2004, *Phys. Rev. D*, 69, 043512
- Pieri L., Branchini E., Hofmann S., 2005, *Phys. Rev. Lett.*, 95, 211301
- Reed D. et al., 2005, *MNRAS* 359, 1537
- Sreekumar P. et al., 1998, *Astrophys. J.*, 494, 523.
- Stoher F. et al., 2003, *MNRAS*, 345, 1313
- Tasitsiomi A., Gaskins J., Olinto A. V., 2004, *Astropart. Phys.*, 21, 637
- Tegmark M. et al., 2006, *Phys. Rev. D*, 74, 123507
- Tyler, C., 2002, *Phys. Rev. D*, 66, 023509
- Ullio P., Bergström L., 1998, *Phys. Rev. D*, 57, 1962
- Ullio P., Zhao H., Kamionkowski M., 2001, *Phys. Rev. D*, 64, 043504
- Zhao H. et al., 2005, *astro-ph/0508215*
- Strigari Louis., Koushiappas S., Bullock J., Kaplinghat., 2007, *Phys. Rev. D*, 75, 083526